CORE Metadata, citation and similar papers at core.ac.uk
Provided by Earth-prints Repository

JOURNAL OF GEOPHYSICAL RESEARCH, VOL. ???, XXXX, DOI:10.1029/,

On the local Hurst exponent of geomagnetic field fluctuations: Spatial distribution for different geomagnetic activity levels

Paola De Michelis[1] and Giuseppe Consolini[2]

Correspondence to: Paola De Michelis, Istituto Nazionale di Geofisica e Vulcanologia, Via di Vigna Murata 605, 00143 Roma, Italia; Phone: +390651860315; Email: paola.demichelis@ingv.it.

[1]Istituto Nazionale di Geofisica e Vulcanologia, 00143, Roma, Italy.

[2]INAF-Istituto di Astrofisica e Planetologia Spaziali, 00133, Roma, Italy.

Abstract. This study attempts to characterize the spatial distribution of the scaling features of the short time scale magnetic field fluctuations obtained from 45 ground based geomagnetic observatories distributed in the northern hemisphere. We investigate the changes of the scaling properties of the geomagnetic field fluctuations by evaluating the local Hurst exponent and reconstruct maps of this index as a function of the geomagnetic activity level. These maps permit us to localize the different latitudinal structures responsible for disturbances and related to the ionospheric current systems. We find that the geomagnetic field fluctuations associated with the different ionospheric current systems have different scaling features, which can be evidenced by the local Hurst exponent. We also find that, in general, the local Hurst exponent for quiet magnetospheric periods is higher than that for more active periods suggesting that the dynamical processes that are activated during disturbed times are responsible for changes in the nature of the geomagnetic field fluctuations.

1. Introduction

It is well known that the magnetic field observed at the Earth's surface is not constant, but subjected to variations on all time scales [*Merrill et al.*, 1996]. Fluctuations with periods from a few tens of minutes up to two hundreds minutes are of primary interest in this study. These fluctuations are the results of both regular and irregular variations related to the interaction between the solar wind and the Earth's magnetosphere. As a result of this interaction a considerable amount of energy is continuously released, giving rise to a number of fast phenomena that occur in the magnetosphere and polar upper atmosphere. Examples include: electric fields, large scale plasma motions, electric currents, aurorae, magnetic substorms and storms, and so on. Within this system, observations of ground-based magnetometer stations can provide an excellent indicator of space weather conditions and thus serve as a remote sensing tool of distant magnetospheric processes. That is consequence of the property of the magnetic field lines to focus and converge as they approach the Earth and consequently to give us the opportunity to see mapped on the Earth all the nonlinear plasma processes that occur in different regions of the magnetosphere. Indeed, the dynamics of the Earth's magnetosphere in response to the solar wind changes is mainly complex, nonlinear and multi-scale [*Tsurutani et al.*, 1990; *Consolini et al.*, 1996; *Consolini and Chang*, 2001; *Sharma et al.*, 2001; *Uritsky et al.*, 2002; *Consolini et al.*, 2005, 2008; *Consolini and De Michelis*, 2014]. Its multi-scale nature, which manifests in the absence of a single characteristic spatial and/or temporal scale in response to the solar wind changes [*Lui et al.*, 2000; *Sitnov et al.*, 2001; *Consolini*, 2002; *De Michelis et al.*, 2012], is widely provided by the scale-invariance of geomagnetic and magnetospheric observations (global and/or in situ time series of magnetic field and plasma parameter measurements).

Our goal in this paper is to capture the essential characteristics of geomagnetic fluctuations at the Earth's surface and at the same time to establish the dynamics of the system responsible of such fluctuations. We characterize changes in the statistics of the geomagnetic field fluctuations evaluating the local Hurst exponent, measured from a single ground-based magnetometer station. This analysis is applied on time interval contains both several days of low geomagnetic activity and a severe magnetic storm. Whereas storms of small or moderate intensity are nothing extraordinary, more severe storms with field depression of about -300 nT are sometimes not observed for years (or even decade) and are thus significant geophysical events. It is the reason why we have selected magnetic data recorded on July, 2000 at 45 geomagnetic observatories in the northern hemisphere. The selected period contains one of the largest historical geomagnetic storms: the Bastille event of 14-16 July 2000.

We use the Hurst exponent for investigation of the essential characteristics of the geomagnetic field fluctuations during different geomagnetic activity levels because this quantity, which is a measure of the way in which a data series varies in time, can be used to obtain significant results on the characterization of the dynamical systems. The Hurst exponent can be used to characterize the persistence of a system, e.g., whether the sign of the fluctuations will remain the same (persistent) or change (anti-persistent) in the next time interval. Since in the case of temporal variations, the geomagnetic field does not exhibit a simple monofractal scaling behavior which can well described as a single scaling exponent, but is often characterised by a scaling behavior which is more complex, it is necessary to introduce different scaling exponents for different parts of the series for a full description of the scaling behavior [*Consolini et al.*, 1996; *Consolini and De Michelis*, 1998; *Sitnov et al.*, 2000, 2001; *Wanliss*, 2005; *Uritsky et al.*, 2002]. In this case, a local fractal analysis must be applied and the time series showing different local scaling features is said to be *multifractional*. If we use the Hurst exponent to characterize the properties of a time series, it will be better to introduce a local Hurst exponent because its scaling properties are not constant. Indeed, it is of extreme importance to correctly quantify the long-range correlations of the geomagnetic time series in order to gain a deep understanding of the complex system dynamics that give rise to the recorded geomagnetic signal.

In recent years, there has been increasing interest in the analysis of the Hurst exponent of geomagnetic signals. However, we have found no studies which analyze the magnetic field fluctuations obtained from a large number of ground based observatories to reconstruct the global temporal and spatial evolution of the local Hurst exponent in order to characterize the scaling features of fluctuations.

The aim of this paper is therefore to investigate the spatial and temporal distribution of the local Hurst exponent in the northern hemisphere, to examine the time evolution of the spatial structure according to different geomagnetic activity levels and to attempt an interpretation of these spatial-temporal fluctuation structures in terms of different ionospheric current systems and convection patterns.

The paper is organized as follows. At first, the data sources are discussed then a brief summary of detrended moving average (DMA) technique to evaluate the local Hurst exponent is presented. Following this, DMA technique is applied to the selected dataset. Finally, the implications of the findings are discussed.

2. Data

The present work focuses on the analysis of the time fluctuations of the Earth's magnetic field from 1^{st} to 31^{st} July 2000. This time interval contains both periods of relatively low geomagnetic activity and periods characterized by the occurrence of intense geomagnetic storms. Indeed, the selected period contains one of the largest historical geomagnetic storms: the Bastille Day event of 14-16 July 2000. It was an extreme space weather event that led to significant damage to satellites and other technological infrastructure. We analyze the scaling features of the horizontal component of the geomagnetic field, as this is mainly affected by magnetospheric dynamics. The dataset is obtained from 45 magnetic observatories distributed in the northern hemisphere. All the selected observatories are part of the worldwide network of observatories known as INTERMAGNET. Therefore, we make use of recordings only obtained by permanent observatories fulfilling international standards. Indeed, the high data quality especially a good stability of instruments guarantees that our targets can be reached. Fig. 1 shows the distribution of the selected observatories in the geomagnetic reference system. The geographical and magnetic coordinates of these observatories, their magnetic local time (MLT), their L-shell values and their International Association of Geomagnetism and Aeronomy (IAGA) codes are listed in Table 1. These quantities for the year 2000 are calculated using NASA-service (*omniweb.gsf.nasa.gov/vitmo/cgm_vitmo.html*). One-minute sampling data have been downloaded either from the World Data Center for Geomagnetism, Edinburgh (*www.wdc.bgs.sc.uk*) or from the INTERMAGNET website (*www.intermagnet.org*).

3. Method of analysis: detrending moving average

To date various methods have been developed and introduced to estimate the generalized Hurst exponent: the rescaled range (R/S) analysis [*Hurst*, 1951], the wavelet transform module maxima (WTMM) approach [*Holschneider*, 1988; *Muzy et al.*, 1991; *Bacry et al.*, 1993; *Muzy et al.*, 1993, 1994], the fluctuation analysis (FA) [*Peng et al.*, 1992], the detrended fluctuation analysis (DFA) [*Peng et al.*, 1995], the detrending moving average (DMA) technique [*Alessio et al.*, 2002], and so on. In our present work, we focus on a moving average method, the so-called DMA technique. This method, which is based on the analysis of the scaling features of the local standard deviation around a moving average, is quite simple and seems to be more accurate than other methods [*Carbone et al.*, 2004]. It is commonly used to quantify signals where large high-frequency fluctuations may mask characteristic low-frequency patterns. Comparing each data point to the moving average, DMA method determines whether data follow the trend, and how deviations from the trend are correlated. In this way, the method addresses the problem of accurately quantifying long-range correlations in non-stationary fluctuating signals.

DMA method consists of the following steps. Let $y(i)$ be a stochastic time series defined in the interval $[0, N]$. This time series $y(i)$ (with $i = 1, 2, ..., N$) is divided into non-overlapping segments of equal length s. Since the length N of the series is often not a multiple of the considered time scale s, a short part at the end of the profile may remain. In order not to disregard this part of the series, the same procedure is repeated starting from the opposite end. Thereby, $2N_s$ ($N_s = int(N/s)$) segments are obtained altogether. For each of the $2N_s$ segments, the first step of DMA method is to detect trends in data employing a moving average, which can be a simple moving average or weighted one. Once the moving average is obtained, the signal is detrended by subtracting the average value of the time series $y(i)$ over each segment. Successively, the fluctuation (i.e. the standard deviation) $F(s)$ of the signal is determined. This last quantity is calculated for different values of the moving average window s over the interval $[s, N]$. It is so possible to obtain the fluctuation function $F(s)$ as function of the scale s and consequently to analyze the relation between these two quantities. If a power law relation between the fluctuation function $F(s)$ and the scale s is found, it will be interpreted as an indication of a self-similar behavior which is obtained for long-memory correlated processes. The power law relation $F(s) \sim s^H$ **allows us to estimate** the local scaling Hurst exponent (H) of the series without any a priori assumption on the stochastic process and on the probability distribution function of the random variables entering the process [*Carbone et al.*, 2004]. From the value of H we have a measure of the long-term memory of the time series and gain some insight into its dynamics. The value of the Hurst exponent let us ascertain whether the analyzed time series has an anti-persistent or persistent behavior. It has been shown that a Hurst exponent value between 0 and 0.5 exists for time series with an *anti-persistent behavior*. This means that an increase will tend to be followed by a decrease (or a decrease will be followed by an increase). Conversely, a Hurst exponent value between 0.5 and 1 indicates a *persistent behavior*, so that an increase (decrease) in values will be followed by an increase (decrease) in the short term - that is, the time series is trending. The larger the Hurst exponent value is, the stronger the trend. Series of this type are easier to predict than series falling in the other category. Lastly, a Hurst exponent value close to 0.5 indicates that there is no correlation in sign between successive increments.

In our work we are interested in the analysis of the geomagnetic fluctuations in the high-frequency domain, which corresponds to a temporal scale lower than 100/200 minutes. This temporal scale characterizes the fast magnetotail relaxation processes associated with the loading-unloading component of the magnetospheric/magnetotail dynamics (see e.g. *Kamide and Kokubun* [1996]; *Consolini et al.* [2005] and references therein). For this reason, in DMA technique we choose a time window of 801 points to ensure an optimal noise/signal ratio in determining the local Hurst exponent. It has been shown by *Consolini et al.* [2013] using a synthetic signal of $5 \cdot 10^5$ points, that for this time window (801 points) the local Hurst exponent estimated using DMA technique can be determined with an average precision equal to 10%. Thus, the selected time window is a good compromise between the time domain of the magnetic fluctuations that we can analyze and the need to have sufficient statistical power for the local Hurst exponent estimation.

4. Analysis and Results

As described in the previous Section, we employ DMA analysis to determine the statistical nature of our signals. We consider a period of one month from 1^{st} to 31^{st} July, 2000 and DMA is used to determine the temporal evolution of the local Hurst exponent evaluated considering the horizontal component (with 1 min resolution) of the Earth's magnetic field measured in the selected 45 permanent geomagnetic observatories reported in Table 1. An example of our results is shown in Fig. 2 where the trend of the local Hurst exponent is presented in the case of nine geomagnetic observatories distributed mainly in Canada. They are nine permanent observatories approximately with the same magnetic longitude and a magnetic latitude ranging between 87° N and 40° N. They are located: three (ALE, RES and CBB) inside the polar cap, three (YKC, BLC and FCC) in the auroral zone and three (MEA, NEW and BOU) immediately below the auroral zone (see Table 1 for details). The position of these observatories offers the opportunity to analyze both areas with a direct influence of the solar wind (where the magnetic field lines are open) and areas where the influence of the solar wind is indirect and the internal magnetosphere dynamics plays a key role.

As shown in Fig. 2 the intermittent character of the analyzed time series is the result of a superposition of structures (set of fluctuations) characterized by different values of the local Hurst exponent. The nature of the signals seems to be very close to that of a multifractional brownian motion [*Lim and Muniandy*, 2000], which is characterized by a non-stationarity of the scale invariance properties. We underline that the *multifractionality* should not be confused with the *multifractality*. In the case of a multifractal signal, the scaling features are function of the fluctuation amplitudes, i.e. of the local crowding of the measure, so that the Hurst exponent depends on the fluctuation amplitudes. Conversely, for a multifractional time series the Hurst exponent is a function of time, i.e. $H = f(t)$. The values of the local Hurst exponent, reported in Fig. 2, are in the interval $[0, 1]$, and consequently, the analyzed time series are characterized at scales below 100 minutes both by fluctuations that tend to induce stability within the system (where the Hurst exponent value is between 0 and 0.5), and by fluctuations with a *persistent behavior*, implying a dynamics governed by a positive feedback mechanism. In the time interval chosen, we select 4 consecutive days characterized by a low geomagnetic activity level (6, 7, 8, and 9 July, 2000) and 4 days during which the Bastille event occurred (from 15 July (14:37) to 19 July (14:36)). We choose the three-hour Kp index to discriminate between different levels of magnetospheric activity. We could use other indices, for example $SYM-H$ or AE, but ranging the magnetic latitude of the selected observatories between 14° N and 87° N, we choose Kp since this index, as a mid-latitude index, would reflect the mean magnetospheric activity. In particular, the days of low activity level correspond to the quietest days of July, 2000. It should be noted that as the general disturbance level may be quite different for different years and also for different months of the same years, the selected quietest days of a month may sometimes be rather disturbed or viceversa. In our case the selected days refer to a value of $Kp < 3$.

These two samples (6 - 9 July and 15 - 19 July) are chosen to better assess the potential of the local Hurst exponent to reveal the transitions in magnetograms during periods characterized by low and disturbed geomagnetic activity levels.

Fig. 3 shows the distributions of the local Hurst exponent values during the Bastille event (from 15 to 19 July, 2000) at the nine different geomagnetic observatories chosen as sample. These probability distribution functions are obtained using a Gaussian kernel method as described in *Kaiser and Schreiber* [2002]. Looking at Fig. 3, there is an increase of anti-persistent behavior of the signal with the decreasing of latitudinal values (from ALE to MEA) which is due to the existence of a greater number of periods characterized by local H values less than 0.5. The three higher latitude stations are consistent with local Hurst exponent distribution shapes centered on local H values greater than 0.5, implying time series characterized by long memory effects. On the contrary, local Hurst exponent distribution shapes centered on local H values lower than 0.5 characterize the geomagnetic observatories, located at lower latitudes (YKC, FCC and MEA). At the end, the other two observatories NEW and BOU, which are located below the auroral zone, show local Hurst exponent value distributions similar to those of the geomagnetic observatories located at higher latitude.

To visualize easily the dependence of the local H values on the latitude we report in Fig. 4 the average values of the local Hurst exponent in the nine selected geomagnetic observatories during both the disturbed period (red markers) and the quiet one (black markers). Fig. 4 reveals that there is a sharp dependence of the Hurst exponent values on the latitude. The Hurst exponent values decrease moving from polar regions to auroral ones and then increase again at mid latitude. The most interesting findings are the position of the minimum, which is different moving from quiet to disturbed periods, and the values of the local Hurst exponent that are lower during disturbed period than quiet one. The dependence of the local Hurst exponent values on the magnetic latitude may be representative of the variability of the auroral electrojet position, namely the variability of that electric current system flowing in the polar ionosphere within the auroral oval. Although the auroral oval is usually located at high latitude, we can observe its expansion towards lower latitudes during very high geomagnetic activity periods as that selected in our present work. Thus, a possible explanation for this result may be the different positions of the low and the high latitude boundary layers where the auroral electrojet flows. A possible explanation of the lower values of the Hurst exponent during disturbed periods than those relative to quiet ones might be the activation of different dynamical processes. Indeed, during a magnetic storm the global ionospheric electric currents and the associated magnetic variations increase in magnitude and exhibit rapid fluctuations. The distributed magnetic perturbations are only partly associated with overhead ionospheric currents, since a substantial portion comes from more distant magnetospheric currents like the ring current and the field-aligned currents. The dynamical processes that are activated during a magnetic storm, produce a change in the nature of the magnetic field fluctuations, which will tend to induce stability within the current systems.

To confirm the above results we report in Fig. 5 and Fig. 6 polar view maps of the local H values computed in each of the selected 45 geomagnetic observatories during different days with a time resolution of 15 minutes. In detail, Fig. 5 shows our results during a quiet day, while Fig. 6 shows our results in five different days during the different phases of the Bastille geomagnetic storm as shown by the $SYM-H$ plot: before, during and after the occurrence of the famous geomagnetic storm (panel a, b, c, d and e). To compute these maps, data are reduced on a regular grid using a weighted Gaussian kernel interpolation scheme. This method gives us the opportunity to use all the available data consisting of the local Hurst exponent values as function of magnetic latitude and magnetic local time and computing the local value on the map averaging with a weight that depends on the distance as a Gaussian function.

The most interesting finding reported in Fig. 5 and Fig. 6 is the spatial distribution of the local H values which shows a dependence on both the magnetic latitude according to the results reported in Fig. 4, and the magnetic local time, showing a noon-midnight asymmetry. Regardless of the geomagnetic activity level, indeed, H values are often higher than 0.5 (blue colour) within the polar cap, i.e. that region where the magnetic field lines stick right out into interplanetary space. However, the structure of the maps reported in Fig. 5 and Fig.6 is completely different. During a geomagnetically quiet day (Fig. 5) the local H values of the magnetic field fluctuations mainly show a persistent character (blue color), except for three different zones. One of these covers the magnetic latitudes from 70° N and 80° N on the morning side. In this case the change of the magnetic field fluctuation character may be due to the presence of the eastward auroral electrojet. The other two zones cover the magnetic latitudes from 20° N and 30° N on the morning side and from 30° N and 50° N on the night side. These two zones correspond to the *solar quiet* or S_q current system. This ionospheric current system is fixed with respect to the Sun and it consists in two vortices on the dayside of the Earth, one in each hemisphere. Seen from the Sun the two vortical currents are counter flowing in the two hemisphere with their center located around 30° north or south magnetic latitude. Furthermore, in the night time hemisphere there are also other two vortices rotating in opposite directions with respect to the dayside ones and characterized by a weaker intensity [*Merrill et al.*, 1996]. Thus, we associate the smaller values of the local H exponent in Fig. 5 with these S_q current ionospheric systems, one in the dayside and the other in the night one. The different H values, which are smaller in the night sector than in the day one, emphasize the more anti-persistent character of the magnetic field fluctuations in the nightside. This suggests that at temporal scales lower than 200 minutes the dayside S_q current is more stable showing no long term coherent variations.

Another important finding is the significant decrease in the values of the Hurst exponent during the development of the analyzed geomagnetic storm as also shown in Fig. 4. Looking at the maps reported in Fig. 6 there is a large decrease in the H values at all magnetic latitudes during the main phase of the storm (panel b) and in the following day (panel c) when the H values reach the absolute minimum of the analyzed disturbed period. Thus, the magnetic fluctuations exhibit a relatively sudden change from more-persistent ($H > 0.5$) to less-persistent pattern ($H < 0.5$) during the analyzed magnetic storm suggesting the establishment of a dynamical phase characterized by anti-persistent fluctuations. This may be related to the presence of a strong coherent electrojet and the anti-persistent nature of short time scale fluctuations may be related to the stability of such current system on longer time scale (long time average of current nearly constant). Consequently, this type of analysis allows us to visualize zones where the stable current systems flow. It is known that the position and the dimension of the auroral electrojet current system is subject to strong temporal variations depending on the geomagnetic activity level. Whereas both the polar cap and polar oval contract to relatively narrow region around the magnetic pole during quiet condition, the diameter of the polar cap and width of polar oval both expand during active conditions. In the strongest magnetospheric storms, as the Bastille event, the auroral electrojets shift equatorward drastically. During the main phase of intense storms, the westward electrojet can cover the latitude from 50° N to 80 °N on the night side while the eastward electrojet flows in the dusk sector at latitudes lower than those of the westward electrojet. With $SYM-H$ varying from 0 to -400 nT, the minimum latitude appeared to lower down from 67° N to 52° N. This accords with our observations. Indeed, panel c) shows the presence of a minimum in the H values between 70° N and 50° N in the morning sector and between 70° N and 60° N in the evening one, which is consistent with the presence of the eastward electrojet in the evening sector and a westward electrojet in the morning one.

5. Summary and Conclusions

The main goal of the current study was to characterize the spatial distribution of the fractal behavior of the short time scale magnetic field fluctuations obtained from 45 ground-based geomagnetic observatories distributed in the northern hemisphere in order to analyze and better understand the complex magnetospheric dynamics in response to the solar wind changes. Since the geomagnetic time series are dominated by multi-scale processes where the scaling exponent is no longer constant but a function of the time, we used a time-dependent approach to find a local measurement of the degree of the long-range correlations described by the temporal variations of scaling exponent. For this reason, the local Hurst exponent was used to study of the scaling properties of the geomagnetic field fluctuations during quiet and disturbed geomagnetic activity levels.

The local Hurst exponent images give us the opportunity to localize the different latitudinal structures caused by different physical processes, and to study their time evolution according to different geomagnetic activity levels. We find that the geomagnetic field fluctuations associated with the different ionospheric current systems have different scaling features, which can be evidenced by the local Hurst exponent. Furthermore, analyzing the features of the geomagnetic field fluctuations we may visualize on our maps structures caused by different physical processes. Processes characterized by a larger value of the Hurst exponent are more regular and less erratic than processes characterized by a smaller one.

We find the emergence of two distinct patterns: a pattern related to the occurrence of intense geomagnetic storms and a pattern related to quiet periods. The first pattern is characterized by a decreasing in the H values, which reaches its minimum near the main phase of the storm, while the second pattern has fluctuations with a more persistent character at scales below 100 minutes. Thus, the geomagnetic field fluctuations change from a more to a less persistent character during the development of a strong geomagnetic storm suggesting the establishment of a dynamical phase characterized by fluctuations with an anti-persistent character at short time scale, which reflect the higher stability of currents at short time scales. On the other hand, during disturbed periods associated with the occurrence of intense geomagnetic storms the complexity and the multi-scale nature of the magnetosphere response to the solar wind forcing is higher than during less active periods [*De Michelis et al.*, 2012], reflecting the different processes that dominate the dynamics of magnetosphere during quiet and disturbed periods. During disturbed periods the magnetospheric dynamic is strongly affected by the impulsive and bursty character of plasma transport in the equatorial magnetotail regions [*De Michelis et al.*, 1999]. This plasma transport process is characterized by a strong intermittent coherent dynamics on short time scales [*Consolini and Chang*, 2001; *Klimas et al.*, 2000]. This might be a possible alternative explanation for the origin of the anti-persistent short time scale fluctuations observed during disturbed periods that can be understood in terms of impulsive local current enhancements. During quiet periods the energy influx from the solar wind is stored in the magnetosphere and slowly burned so to generate a more long time correlated variation of current systems. That is the possible origin of the persistent character of the fluctuations at short time scale observed during these periods. These seem still to be consequence of a stochastic dynamics, similar to the global dynamics that is characterized by a long-varying Markovian non-equilibrium relaxation process (see e.g. *de Groot and Mazur* [1984]).

The findings of the current study seem to be different from those obtained in previous research. In some published studies a transition from a random to a correlated state is actually observed and discussed during the active periods of storms in the *Dst* index

[*Balasis et al.*, 2006] and the $SYM-H$ index [*Wanliss*, 2005; *Wanliss and Dobias*, 2007]. These differences may be explained considering some important points:

i) previous works [*Wanliss*, 2005; *Balasis et al.*, 2006; *Wanliss and Dobias*, 2007] use time series of the geomagnetic indices for obtaining their results. This means that they use time series calculated as an average of mid-latitude geomagnetic observatories after taking into account the secular variation and the system of the external S_q currents at each location. In contrast, here, the observatory data, to which DMA was applied, are raw measurements;

ii) Balasis et al. [2006] and *Zaourar et al.* [2013] use hourly data whereas we use 1 minute resolution data;

iii) Hurst calculations by *Balasis et al.* [2006] and *Zaourar et al.* [2013] are made using wavelet transform in the frequency domain. They estimate power spectral densities in the time scale range from 2 to 128 hours, thus looking overall at longer period processes in the magnetosphere than the present study.

However, by monitoring the temporal evolution of the fractal character in their time series, a rapid change in their temporal scaling is found around the beginning of the main phase of the geomagnetic storms. This finding is also supported by *Zaourar et al.* [2013], where the dynamics of the external contributions to the geomagnetic field is investigated by applying time-frequency methods to magnetic data recorded at three geomagnetic observatories. Looking at their results we notice that during quiet times the values of the spectral exponent β (where $\beta = 2H + 1$) are higher than during disturbed times, supporting our findings. Thus, if it is true that we have an increase of the scaling exponent values towards more persistent values around the beginning of the main phase of the geomagnetic storms at mid-latitudes, it is also true that during the overall disturbed period the observed H values decrease towards less persistent and/or anti-persistent values. Thus, our findings provide evidence of the occurrence of a dynamical phase transition, which occurs during the intense geomagnetic storms. This dynamical phase transition manifests by a change of the persistent character of temporal-spatial fluctuations.

In conclusion, this study shows the occurrence of dynamical changes in the fluctuation scaling features on global scale and provides a clear correlation between these scaling features and the current systems flowing in the ionosphere.

Acknowledgments. The results presented in this paper rely on public data collected at magnetic observatories and available by INTERMAGNET (www.intermagnet.org). We thank the national institutes that support them and INTERMAGNET for promoting high standards of magnetic observatory practice. The authors kindly acknowledge N. Papitashvili and J. King at the National Space Science Data Center of the Goddard Space Flight Center for the use permission of 1-min OMNI data and the NASA CDAWeb team for making these data available. Giuseppe Consolini acknowledges funding from the European Community's Seventh Framework Programme ([FP7/2007-2013]) under Grant no. 313038/STORM. The elaborated data for this paper are available by contacting the corresponding author (paola.demichelis@ingv.it).

References

Alessio E., A. Carbone, G. Castellli, and V. Frappietro (2002), Second-order moving average and scaling of stochastic time series, *Eur. Phys. J.*, *B 27*, 197-200.

Bacry, E., J. F. Muzy, and A. Arnéodo (1993), Singularity spectrum of fractal signals from wavelet analysis: Exact results, *J. Stat. Phys.*, *70*, 635-674.

Balasis G., I. A. Daglis, P. Kapiris, M. Mandea, D. Vassiliadis, and K. Eftaxias (2006), From pre-storm activity to magnetic storms: a transition described in terms of fractal dynamics, *Ann. Geophys.*, 24, 3557.

Carbone, A., G. Castelli, and H. E. Stanley (2004), Time-dependent Hurst exponent in financial time series, *Physica A*, *344*, 267-271.

Consolini G., M. F. Marcucci, and M. Candidi (1996), Multifractal structure of auroral electroject index data, *Phys. Rev. Lett.*, *76*, 4082.

Consolini G., and P. De Michelis (1998), Non-Gaussian distribution function of AE-index fluctuations: evidence for time intermittency, *Geophys. Res. Lett.*, *25*, 4087.

Consolini G., and T. Chang (2001), Magnetic field topology and criticality in geotail dynamics: relevance to substorm phenomena, *Space Sci. Rev.*, *95*, 309.

Consolini G. (2002), Self-organized criticality: a new paradigm for the magnetotail dynamics, *Fractals*, *10*, 275.

Consolini G., T. Chang, and A. T. Y. Lui (2005), Complexity and topological disorder in the Earth's magnetotail dynamics, in *Nonlinear transitions in plasma*, Sharma A. S. and P. Kam (eds.), Kluwer.

Consolini, G., and P. De Michelis (2005), Local intermittency measure analysis of AE index: The directly driven and unloading component, *Geophys. Res. Lett.*, *32*, L05101, doi:10.1029/2004GL022063.

Consolini G., P. De Michelis, and R. Tozzi (2008), On the Earth's magnetospheric dynamics: nonequilibrium evolution and the fluctuation theorem, *J. Geophys. Res.*, *113*, A8, doi:10.1029/2008JA013074.

Consolini G., R. De Marco, and P. De Michelis (2013), Intermittency and multifractional Brownian character of geomagnetic time series, *Nonlin. Processes Geophys.*, *20*, 455-466, doi: 10.5194/npg-20-455-2013.

Consolini G. and P. De Michelis (2014), Permutation entropy analysis of complex magnetospheric dynamics, *J. Atm Sol. Terr. Physics*, *115*, 25, doi: 10.1016/j.jastp.2013.11.005

De Michelis P., I. A. Daglis, and G. Consolini (1999), An average image of proton plasma pressure and the ring current systems in the equatorial plane derived from AMPTE/CCE-CHEM measurements, *J. Geophys. Res.*, *104*, 28615.

De Michelis P., G. Consolini, and R. Tozzi (2012), On the multi-scale nature of large geomagnetic storms: an empirical mode decomposition analysis, *Nonlin. Processes Geophys.*, *19*, 667, doi: 10.5194/npg-19-667-2012.

de Groot S.R. and P. Mazur (1984), *Non-equilibrium. Thermodynamics*, Dover, New York.

Holschneider, M. (1988), On the wavelet transformation of fractal objects' *J. Stat. Phys.*, *50*, 963-993.

Hurst, H. E. (1951), Long-term storage capacity of reservoirs, *Trans. Amer. Soc. Civil Eng.*, *116*, 770-808.

Kaiser A., and T. Schreiber (2002), Information transfer in continuous processes, *Physica D*, *166*, 43, doi: 10.1016/S0167-2789(02) 00432-3.

Kamide, Y., and S. Kokubun (1996), Two-component auroral electrojet: Importance for substorm studies, *J. Geophys. Res.*, *101*, 13027.

Klimas A. J., J. A. Valdivia, D. Vassiliadis, D. N. Baker, M. Hesse, and J. Takalo (2000), Self-organized criticality in the substorm phenomena and its relation to localized reconnection in the magnetospheric plasma sheet, *J. Geophys. Res.*, *105*, 18765.

Lim, S.C., and S. V. Muniandy (2000), On some possible generalizations of fractional Brownian motion, *Phys. Lett. A.*, *266*, 140.

Lui A. T. Y., S. Chapman, K. Liou, P.T. Newell, C. I. Meng, M. Brittnacher, and G-K. Parks (2000), Is the dynamic magnetosphere an avalancing system?, *Geophys. Res. Lett.*, *27*, 911.

Merrill R.T., M. W. McElhinny, and P. L. McFadden (1996), *The Magnetic Fields of the Earth. Paleomagnetism, the Core and the Deep Mantle*, Academic Press.

Muzy, J. F., E. Bacry, and A. Arnéodo (1991), Wavelets and multifractal formalism for singular signals: Application to turbulence data, *Phys. Rev. Lett.*, *67*, 3515-3518.

Muzy, J. F., E. Bacry, and A. Arnéodo (1993), Multifractal formalism for fractal signals: The structure-function approach versus the wavelet-transform modulus-maxima method, *Phys. Rev. E*, *47*, 875-884.

Muzy, J. F., E. Bacry, and A. Arnéodo (1994), The multifractal formalism revisited with wavelets, *Int. J. Bifurcat. Chaos*, *4*, 245-302.

Peng, C.-K. et al. (1992), Long-range correlations in nucleotide sequences, *Nature*, *356*, 168-170.

Peng, C.-K. et al. (1995), Mosaic organization of DNA nucleotides, *Phys. Rev. E*, *49*, 1685.

Sharma A. S., M. I. Sitnov, and K. Papadopoulos (2001), Substorms as nonequilibrium transitions of the magnetosphere, *J. Atmos. Sol. Terr. Phys.*, *63*, 1399.

Sitnov M.I., A. S. Sharma, K. Papadopoulos, D. Vassiliadis, J. A. Valdivia, A. J. Klimas, and D. N. Baker (2000), Phase transition-like behavior of the magnetosphere during substorms, *J. Geophys. Res.*, *105*, 12955.

Sitnov M.I., A. S. Sharma, K. Papadopoulos, D. Vassiliadis, J. A. Valdivia, A. J. Klimas, and D. N. Baker (2001), Modelling substorm and self-organized criticality to nonequilibrium phase transitions, *Phys. Rev. E*, *65*, 016116.

Tsurutani B. et al. (1990), The nonlinear response of AE to the IMF Bs, *Geophys. Res. Lett.*, *17*, 279.

Ukhorskiy A.Y., M. I. Sintov, A. S. Sharma, and K. Papadopoulos (2004), Global and multiscale dynamics of the magnetosphere, *Geophys. Res. Lett.*, *31*, L08802, doi: 10.1029/2003GL018932.

Uritsky V. M., A. J. Klimas, D. Vassiliadis, D. Chua, and G. D. Parks (2002), Scale free statistics of spatiotemporal auroral emissions as depicted by POLAR UVI images: The dynamic magnetosphere is an avalanching system, *J. Geophys. Res.*, *107*, 1426.

Wanliss J. A. (2005), Fractal properties of SYM-H during quiet and active times, *J. Geophys. Res.*, *110*, doi:10.1029/2004JA010544.

Wanliss, J. A., and K. Showalter (2006), High-resolution global storm index: Dst versus SYM-H, *J. Geophys. Res.*, *111*, doi: 10.1029/2005JA011034.

Wanliss J.A., and P. Dobias (2007), Space storm as a phase transition, *J. Atmos. Sol. Terr. Phys.*, *69*, 675.

Zaourar N., M. Hamoudi, M. Mandea, G. Balasis, and M. Holschneider (2013), Wavelet-based multiscale analysis of geomagnetic disturbance, *Earth Planets Space*, *65*, 1525.

Table 1. Geomagnetic observatories considered in this study. Geographyical and corrected magnetic coordinates are given in degrees. MLT is given in UT (hours) at time when given point is at midnight. L-shell is given in Earth's radii R_E. Stars indicate a selected number of geomagnetic observatories, that we use in Figs. 2, 3 and 4.

IAGA code	Lat	Long	MLat	MLong	MLT	L-shell
ALE*	82.50	297.65	87.08	99.42	21.76	∞
AQU	42.38	13.32	36.24	87.38	22.39	1.5
BDV	49.08	14.02	44.45	89.56	22.26	1.97
BEL	51.84	20.79	47.57	96.17	21.80	2.20
BLC*	64.32	263.99	73.92	327.50	6.84	13.08
BMT	40.30	116.20	34.57	188.75	16.45	1.48
BOU*	40.14	254.76	49.04	319.61	7.36	2.33
BRW	71.30	203.38	70.04	251.24	12.20	8.6
BSL	30.35	270.36	41.33	340.30	6.07	1.78
CBB*	69.12	254.97	77.25	308.85	7.93	∞
CLF	48.23	2.26	43.51	79.43	23.02	1.92
ESK	55.31	356.79	52.71	77.42	23.23	2.73
FCC*	58.76	265.91	68.92	332.25	6.56	7.75
FRD	38.21	282.63	49.14	375.72	5.08	2.35
FUR	48.17	11.28	43.37	86.90	22.45	1.90

Table 1. (continued)

IAGA code	Lat	Long	MLat	MLong	MLT	L-shell
GUI	28.32	343.56	14.39	60.65	0.49	1.07
HON	21.32	202.00	21.40	269.82	11.13	1.16
HRB	47.87	18.19	43.02	92.89	22.02	1.88
IRT	52.17	104.45	47.32	117.25	17.12	2.18
KAK	36.23	140.19	29.25	211.70	15.06	1.32
KNY	31.42	130.88	24.67	202.80	15.58	1.21
LER	60.14	358.81	58.03	81.18	22.96	3.57
LNP	25.00	121.17	18.22	192.92	16.13	1.11
LRV	61.18	338.3	61.80	65.30	0.34	4.48
MEA∗	54.62	246.65	62.08	305.70	8.17	4.58
MID	28.21	182.62	24.72	249.95	12.44	1.22
MMB	43.91	144.19	37.08	215.46	14.88	1.58
NAQ	61.18	314.58	66.21	43.40	2.14	6.17
NCK	47.63	16.72	42.71	91.45	22.11	1.86
NEW∗	48.27	242.88	54.93	303.27	8.38	3.04
NGK	52.07	12.68	47.95	89.17	22.29	2.24
NUR	60.51	24.66	56.90	102.26	21.39	3.36
OTT	45.40	284.45	55.98	1.05	4.92	3.20
RES∗	74.69	265.12	83.51	319.07	7.30	∞
SIT	54.06	135.33	47.95	207.10	15.46	2.24
SOD	67.37	26.63	63.90	101.37	21.05	5.19
SPT	39.55	355.65	32.40	72.02	23.57	1.41

Table 1. (continued)

IAGA code	Lat	Long	MLat	MLong	MLT	L-shell
STJ	47.59	307.32	53.63	31.28	3.02	2.85
SUA	44.68	26.25	39.52	99.53	21.57	1.69
THY	46.90	17.90	41.88	92.32	22.05	1.81
TRO	69.66	18.95	66.63	103.03	21.36	6.38
VAL	51.93	349.75	49.36	70.52	23.78	2.36
VIC	48.52	236.58	53.80	269.12	8.88	2.88
WNG	53.74	9.07	50.01	86.70	22.49	2.43
YKC*	62.48	245.52	69.50	300.48	8.49	8.18

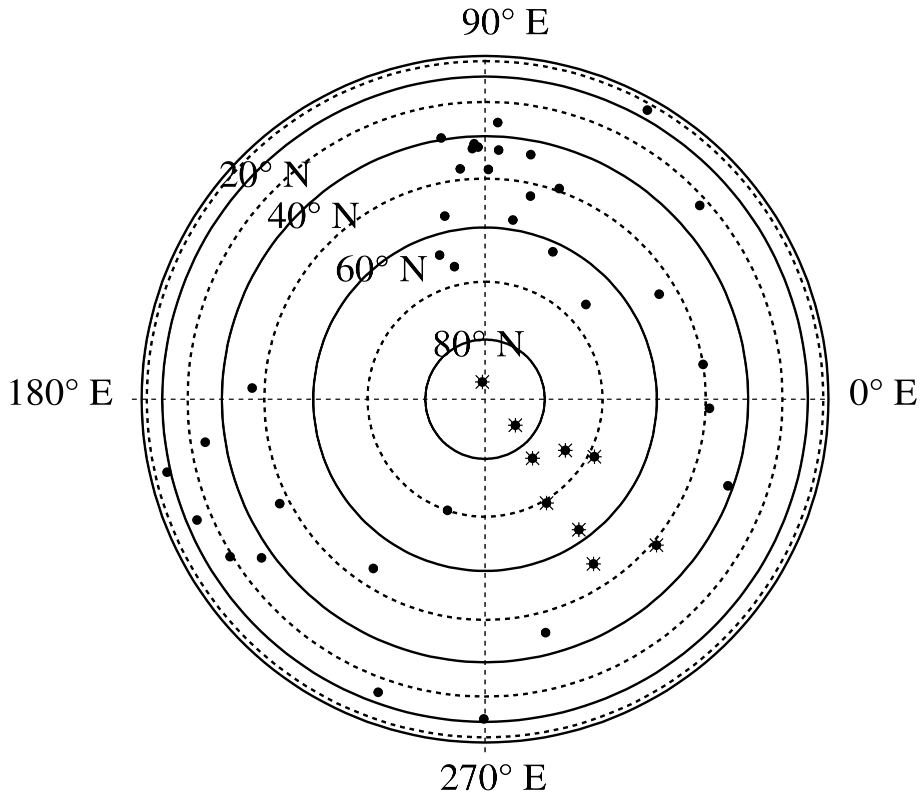

Figure 1. Distribution of the 45 geomagnetic observatories used in the analysis. Magnetic latitude contours are spaced by 10°. Stars indicate the geomagnetic observatories used in Figs. 2, 3 and 4.

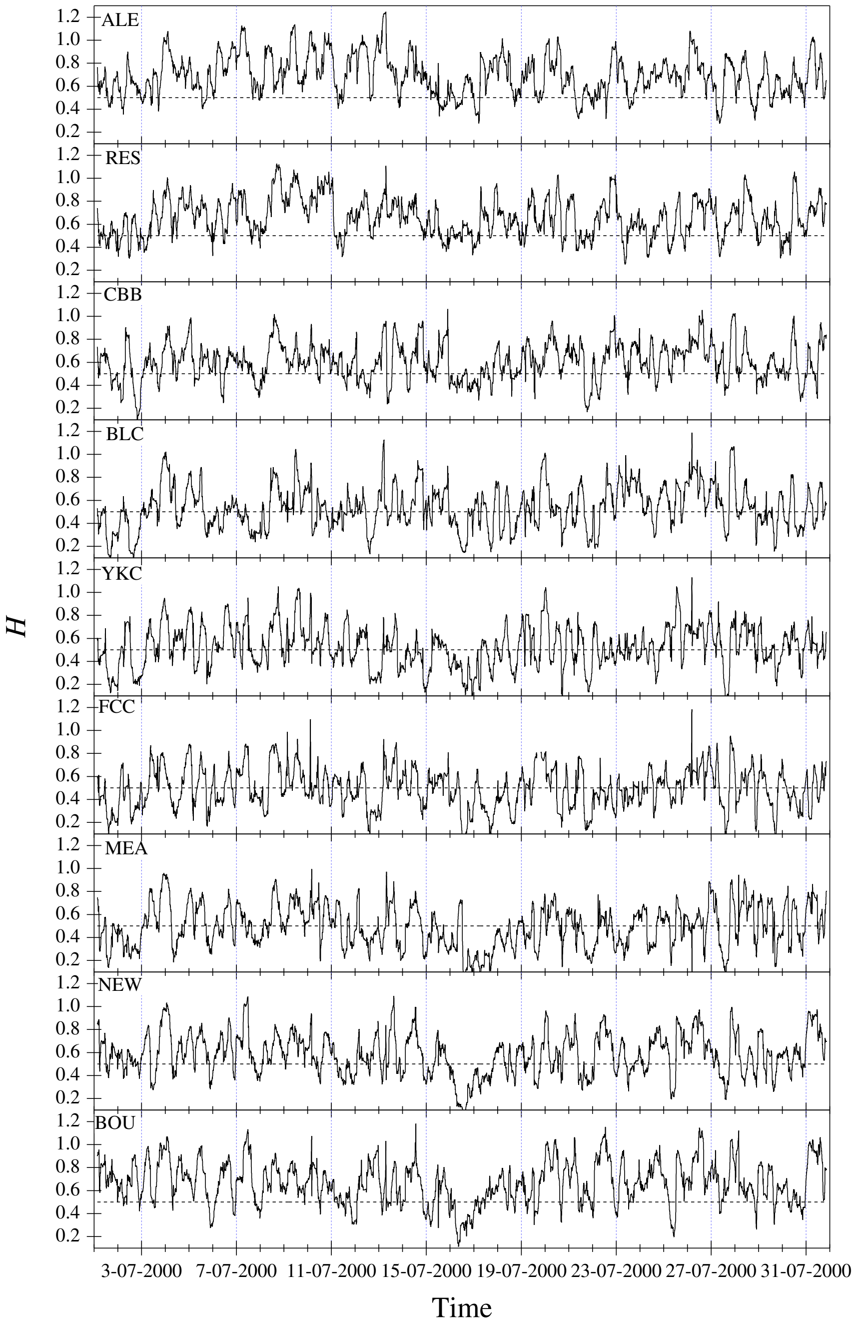

Figure 2. Temporal behaviour of the local Hurst exponent evaluated applying DMA technique on the geomagnetic field horizontal component (with 1 minute time resolution) as collected at nine different observatories during July 2000.

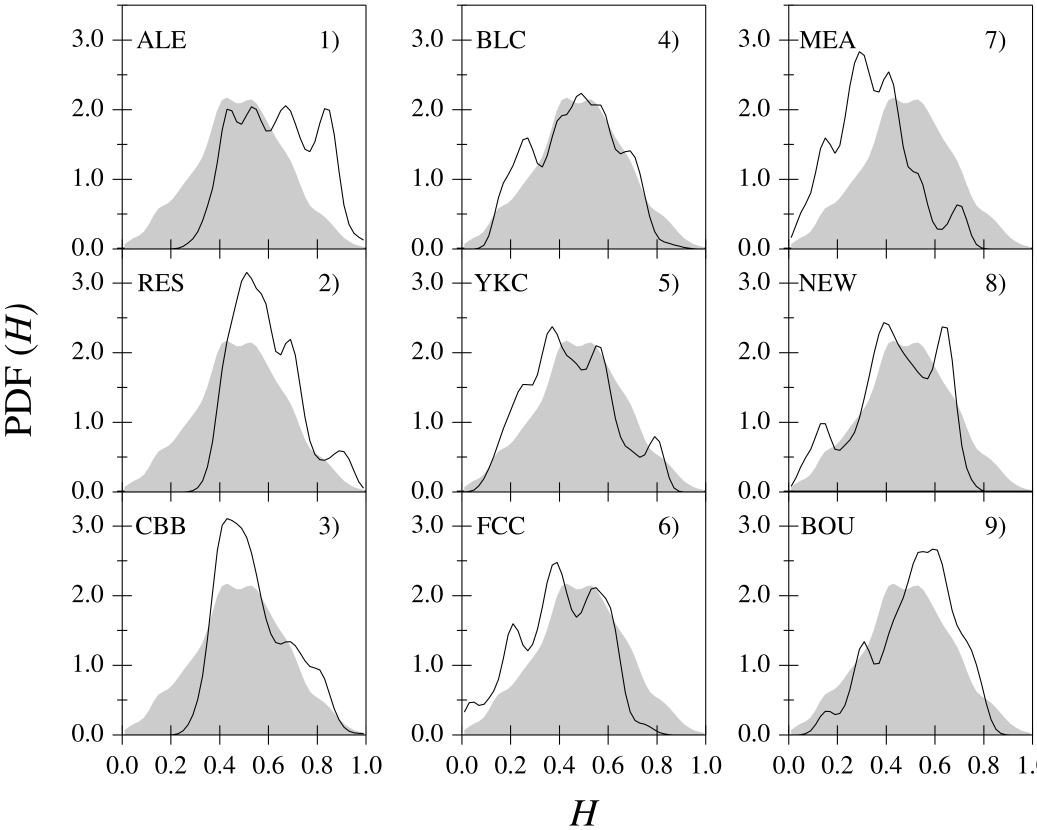

Figure 3. Probability distribution functions (PDFs) of the local Hurst exponent values during the Bastille event (from 15 to 19 July, 2000) at the same nine geomagnetic observatories reported in Fig. 2. The grey PDF in the background is the average one. The plots are reported according to the decreasing value of the geomagnetic observatory latitude (from 1 to 9).

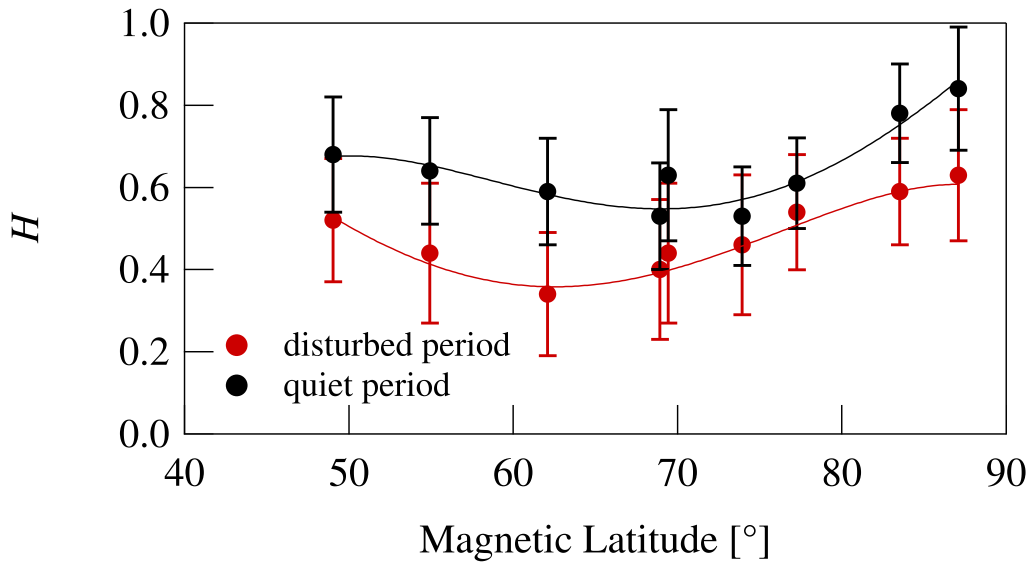

Figure 4. Average values of the local Hurst exponent at the same nine geomagnetic observatories reported in Fig. 2 during both a disturbed period (red markers) and a quiet one (black markers).

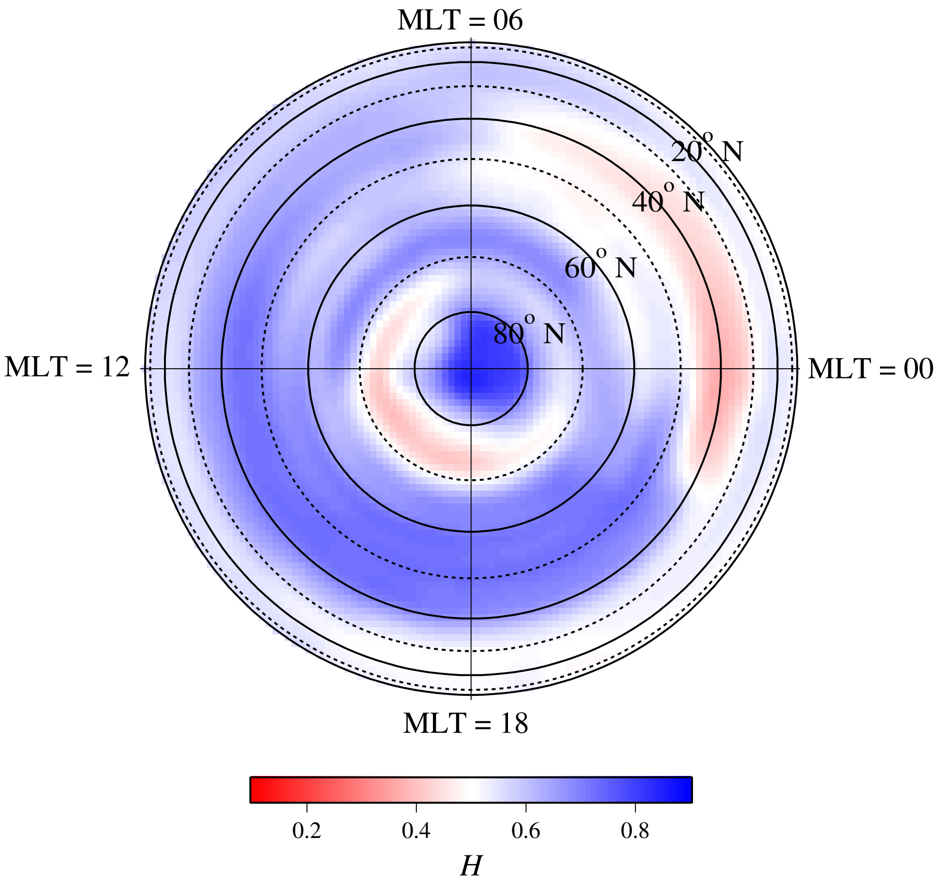

Figure 5. Polar view map of the local Hurst exponent values (H) over the northern hemisphere. The map is relative to July 6, 2000, which is a quiet day. The coordinates are magnetic latitude, from 0° to the North pole, and the magnetic local time (MLT), with local noon at the left side.

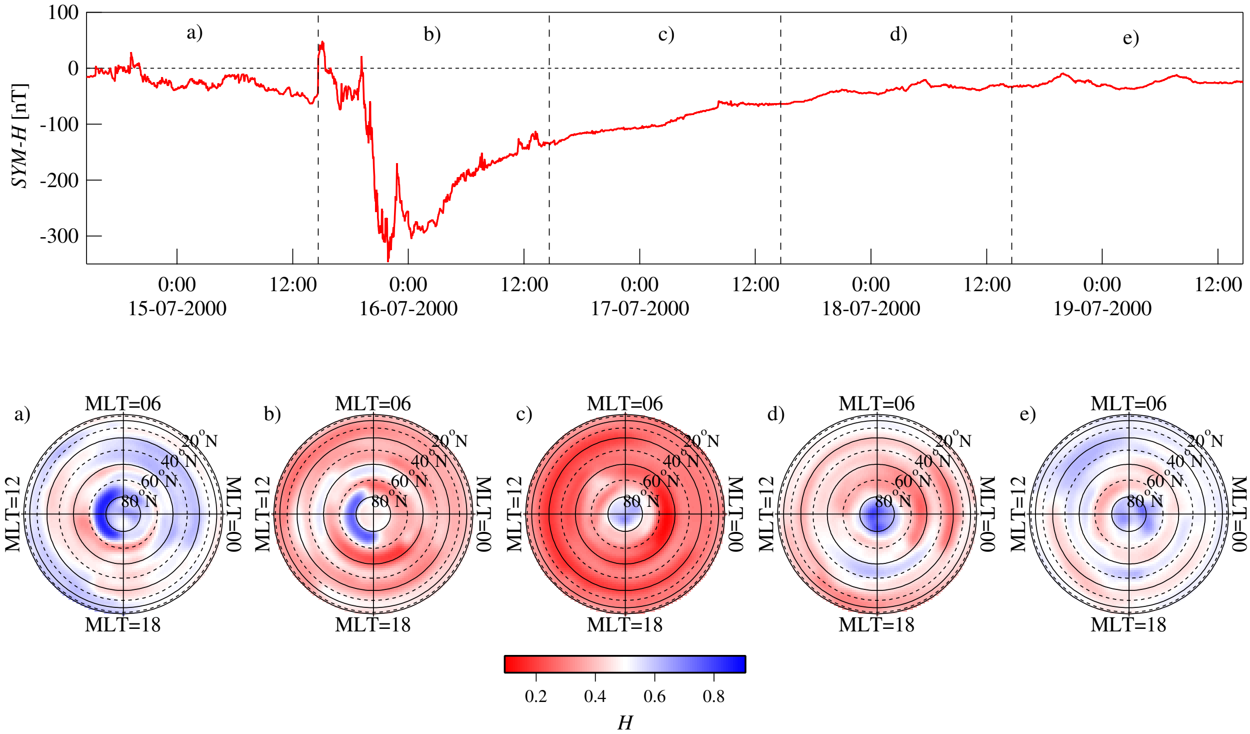

Figure 6. Polar view maps of the local Hurst exponent values (H) during the period characterized by the occurrence of the Bastille event (from14 to 19 July, 2000) on the northern hemisphere. On the top the $SYM-H$ values for the same period. Each polar map corresponds to a day, which is delimited by a dashed line in the $SYM-H$ plot. The coordinates are magnetic latitude, from 0° to the North pole, and the magnetic local time (MLT), with local noon at the left side.